BULLETIN OF THE POLISH ACADEMY OF SCIENCES
TECHNICAL SCIENCES, Vol. 68, No. 2, 2020
DOI: 10.24425/bpasts.2020.133109

Grid-tied converter operated under unbalanced and distorted grid voltage conditions

A. GAŁECKI*, M. MICHALCZUK, A. KASZEWSKI, B. UFNALSKI, and L. M. GRZESIAK

Warsaw University of Technology, ul. Koszykowa 75, 00-662 Warsaw, Poland

Abstract. The paper presents a three-phase grid-tied converter operated under unbalanced and distorted grid voltage conditions, using a multi-oscillatory current controller to provide high quality phase currents. The aim of this study is to introduce a systematic design of the current control loop. A distinctive feature of the proposed method is that the designer needs to define the required response and the disturbance characteristic, rather than usually unintuitive coefficients of controllers. Most common approach to tuning a state-feedback controller use linear-quadratic regulator (LQR) technique or pole-placement method. The tuning process for those methods usually comes down to guessing several parameters. For more complex systems including multi-oscillatory terms, control system tuning is unintuitive and cannot be effectively done by trial and error method. This paper proposes particle swarm optimization to find the optimal weights in a cost function for the LQR procedure. Complete settings for optimization procedure and numerical model are presented. Our goal here is to demonstrate an original design workflow. The proposed method has been verified in experimental study at a 10 kW laboratory setup.

Key words: grid-tied converter, AC/DC converter, current controller, resonant controller, particle swarm optimization.

1. Introduction

Elimination of grid current distortion, understood as current unbalance and high content of higher harmonics, is a major area of interest in the field of control of power electronic converters operating under distorted voltage conditions [1–7]. Generally, the frequency spectrum of grid voltage disturbances is recognized. In three-phase three-wire systems, dominant higher harmonics appearing in grid voltage are 5th, 7th, 11th and 13th [4]. This regularity has consequences in the standards that define the maximum allowable percentage share of these harmonics in grid voltage [8]. Control systems of grid-tied converters are expected to provide a low content of higher current harmonics as well as reliable and safe operation in case of unbalanced and distorted grid voltage conditions. The recommendation regarding the quality of grid current is described in the IEC standards [9, 10].

Two main approaches to cope with periodic disturbances for grid connected converters include the concept of repetitive control or control structures with oscillatory terms (resonant controllers). Examples of implementation of the repetitive controller for AC/DC converters are presented in [11–13] and an attempt to compare these approaches is given in [6, 14]. A slightly different approach based on the virtual electromagnetic torque has been proposed in [15, 16]. Another one based on the model predictive control was shown in [17, 18].

Considering the fact that the number of dominant grid voltage harmonics is limited, it is convenient to create a disturbance model with oscillatory terms selected for given pulsatances. The disturbance model applied in the controller structure allows to discard harmonics with the pulsatance of selected oscillators. Usually, the range of higher harmonics compensation is limited to the 13th harmonic, due to the trade-off between computational complexity and the quality of the obtained current. For the state feedback control structure two analytical approaches, either pole placement [19–21] or LQR (linear quadratic regulator) [22, 23], are predominant. The pole placement method is labour intensive and does not take the control effort directly into account. Assurance of a proper and reasonable control signal is an additional burden for the designer. In contrast, LQR is an optimal multivariable feedback control approach that minimizes excursion in trajectories of state variables, at the same time securing minimum control effort. Thus LQR enhances stability performance and in comparison to the pole placement method, it requires less involvement of the designer [24]. The main concern is the parametric cost function of the LQR procedure. Two penalty matrices **Q** and **R**, to be selected by the designer, related to state variables and control signals respectively, are involved in the cost function. Iterative tuning of LQR by trial-and-error method is usually used [25]. The larger the number of state variables is, the more problematic the selection of **Q** and **R** matrices.

Many methods of selecting weighting matrices based on upper stage optimizers have been presented in literature to overcome the weighting matrices selection problem of a linear quadratic regulator. These methods include, i.a., ant colony optimization [26], artificial bee colony [27], and genetic algorithm

*e-mail: andrzej.galecki@ee.pw.edu.pl

Manuscript submitted 2019-10-11, revised 2019-11-29, initially accepted for publication 2019-12-20, published in April 2020

[28]. In the power electronics area, particle swarm optimization for a voltage-source inverter [29] and genetic algorithm for static synchronous compensator have been implemented [30]. These types of solutions have not been presented for grid connected converters. So far, there are no solutions introducing the cost function that do not require guessing of parameters.

In our previous publications the multi-oscillatory current controller applied for a grid-tied converter has been covered only in the basic approach [31]. The synthesis of the control system with linear-quadratic regulator have been presented for the case, in which selections of the **Q** and **R** matrix coefficients have been set by trial and error approach. Aforementioned strategy has been expanded with an supporting algorithm to limit the state signals of the current controller [32, 33]. Despite considerable effort spent at the tuning stage of the **Q** and **R** matrix parameters the steady-state input currents of the converter obtained with this method were far from optimal. Therefore, the two step evolutionary optimization supported process has been proposed in order to improve tuning of the current controller. The preliminary simulation of a selected simple model based cases have been presented in [34]. In this paper, novel, full analysis of the mentioned two-step approach supported by experimental results from the test bench is provided.

This paper presents evolutionary optimization [35, 36] to facilitate tuning the current controller for a grid-tied converter. PSO has been applied to find weighting matrices for the LQR procedure. The only knowledge required here is basic awareness of the desirable dynamics of the system and the expected level of disturbances. The two-stage optimization using LQR and PSO was chosen in order to provide the design convenience. LQR has been identified as being robustness [37, 38]. Dropping the LQR stage and applying direct selection of feedback gains by PSO, requires an including robustness issues in the PSO cost function, which additionally burdens the designer. This subject has been addressed in the case of PSO tuned PID controller in [39]. It should be added that a time needed for LQR calculation has negligible impact on total time needed to perform proposed two-stage optimization processes. Major impact on optimization time has the number of test cycles required to be evaluated during the optimization. The diagonal **Q** matrix allows to reduce the search-space dimension, which positively affects a computational effort. Moreover, due to the coupling between d and q axes in the AC/DC converter model described in the rotating reference frame, the number of sought parameter is at least two times larger, if the direct tuning state feedback controller is carried out.

2. The control system

This study involves a three-phase three-level neutral point clamped grid-tied converter. The proposed control structure, presented in Fig. 1, is based on voltage oriented control [40].

The inner grid current control loop consists of LQR (Fig. 2). The outer voltage control loop includes a proportional-integral (PI) controller. In order to ensure a maximum linear range a pulse width modulation with triple harmonic zero-sequence signal (TH-ZSS-PWM) is used. The scaling gains k_i and k_{dc} are used to obtain a per-unit control system.

Control of phase currents is accomplished by controlling the current vector in the two rotating coordinates d, q. The current feedback signals are transformed to the synchronous frame using a phase lock loop (PLL) [41]. This way, the current components i_d and i_q controlled by LQR are synchronized with the positive-sequence rotating reference frame with the frequency equal to the fundamental harmonic of the grid voltage. The orthogonal currents components i_d and i_q are related to the active and reactive power on the AC side respectively. The current controller is equipped with oscillatory terms to obtain a nearly sinusoidal shape and balanced grid currents under unbalanced and distorted grid voltage. In order to convert the control system from the continuous to the discrete domain, the Tustin approximation with pre-warping is used [42].

2.1. Linear-quadratic controller. For the purposes of a current controller design, v_{DC} is assumed to be V_{DC}= const. and the state-space model of the system is described in the rotating reference frame as follows [40, 43]:

$$\begin{cases} \dfrac{\mathrm{d}}{\mathrm{d}t}\mathbf{x} = \mathbf{A}\mathbf{x} + \mathbf{B}\mathbf{u} + \mathbf{E}\mathbf{v} \\ \mathbf{y} = \mathbf{C}\mathbf{x} + \mathbf{D}\mathbf{u} \end{cases} \tag{1}$$

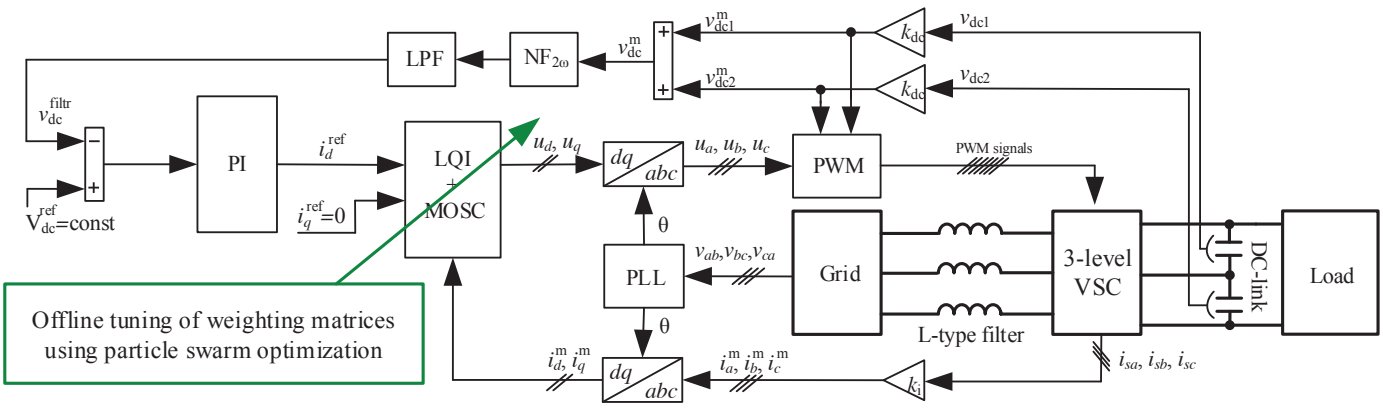

Fig. 1. Control scheme for a grid-tied converter

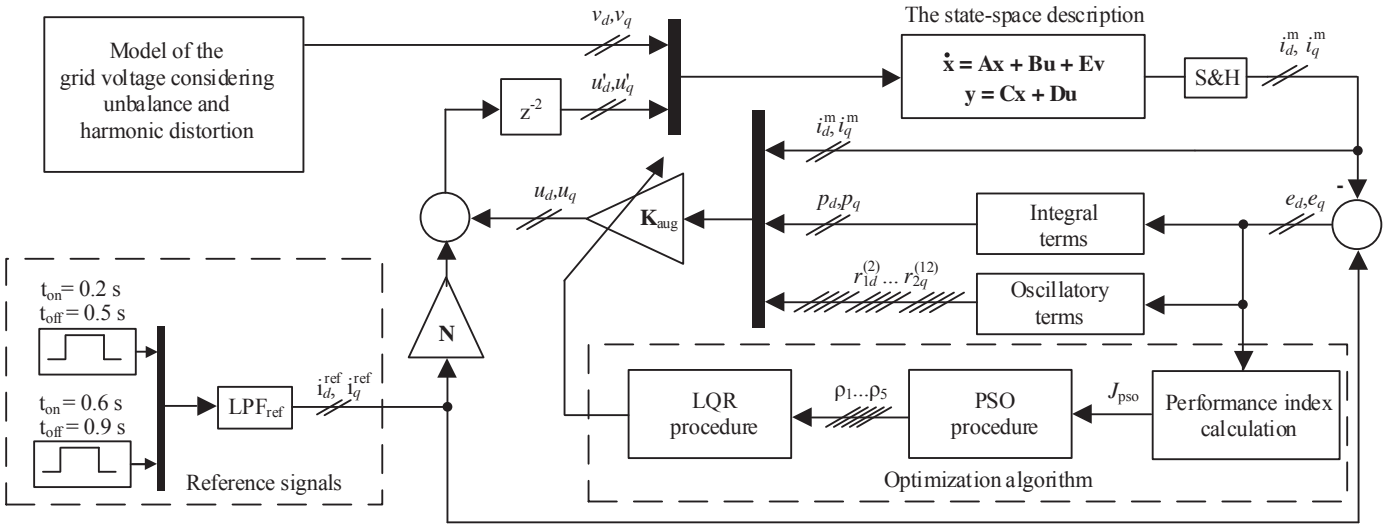

Fig. 2. Schematic diagram of the numerical model with PSO optimizer

where

$$\mathbf{A} = \begin{bmatrix} -\frac{R}{L} & \omega \\ -\omega & -\frac{R}{L} \end{bmatrix}, \qquad \mathbf{x} = \begin{bmatrix} i_d^{\mathrm{m}} \\ i_q^{\mathrm{m}} \end{bmatrix},$$

$$\mathbf{B} = \begin{bmatrix} -\frac{\mathrm{V_{DC}}}{L} k_i & 0 \\ 0 & -\frac{\mathrm{V_{DC}}}{L} k_i \end{bmatrix}, \qquad \mathbf{u} = \begin{bmatrix} u_d \\ u_q \end{bmatrix},$$

$$\mathbf{E} = \begin{bmatrix} \frac{1}{L} k_i & 0 \\ 0 & \frac{1}{L} k_i \end{bmatrix}, \qquad \mathbf{v} = \begin{bmatrix} v_d \\ v_q \end{bmatrix},$$

$$\mathbf{C} = \mathbf{I}_{2\times 2}, \qquad \mathbf{D} = \mathbf{0}_{2\times 2}.$$

The state vector consists of two state signals i_d^{m} and i_q^{m} and the control vector $\mathbf{u}$ consists of two control signals u_d and u_q. Two disturbance signals v_d and v_q are collected in the disturbance vector $\mathbf{v}$. There are five matrices in the state-space model: $\mathbf{A}$ – state matrix, $\mathbf{B}$ – control matrix and $\mathbf{E}$ – disturbance matrix, $\mathbf{C}$ – output matrix and $\mathbf{D}$ – feed–forward matrix.

In order to reduce the constant and sinusoidal component of the error in current tracking caused by voltage distortion, integral and oscillatory terms are incorporated. They can be described as:

$$\frac{\mathrm{d}}{\mathrm{d}t} p_x = e_x, \tag{2}$$

$$\frac{\mathrm{d}}{\mathrm{d}t} r_{1x}^{(h)} = r_{2x}^{(h)}, \tag{3}$$

$$\frac{\mathrm{d}}{\mathrm{d}t} r_{2x}^{(h)} = e_x - (h\omega)^2 r_{1x}^{(h)} - 2\zeta h\omega r_{2x}^{(h)}, \tag{4}$$

where $e_x = i_x^{\mathrm{ref}} - i_x^{\mathrm{m}}$, subscript $x = \{\mathrm{d}, \mathrm{q}\}$, $h = \{2, 6, 12\}$ denotes a selected harmonic order and ζ is the damping factor set at the same level for all selected oscillatory terms [44]. The i_d^{ref} and i_q^{ref} are the reference signals for the current controller. The compensation of the second, the sixth and the twelfth harmonic of the grid currents represented in the d–q rotating frame results in the compensation of unbalance and the fifth, the seventh, the eleventh and the thirteenth harmonic in the natural frame [3].

The state equation for the augmented system in synchronously RRF is given as follows:

$$\frac{\mathrm{d}}{\mathrm{d}t} \mathbf{x}_{\mathrm{aug}} = \mathbf{A}_{\mathrm{aug}} \mathbf{x}_{\mathrm{aug}} + \mathbf{B}_{\mathrm{aug}} \mathbf{u} + \mathbf{E}_{\mathrm{aug}} \mathbf{v}, \tag{5}$$

where

$$\mathbf{A}_{\mathrm{aug}} = \begin{bmatrix} \mathbf{A}_0 & \mathbf{0}_{4\times4} & \mathbf{0}_{4\times4} & \mathbf{0}_{4\times4} \\ \mathbf{A}_{1(2)} & \mathbf{A}_{2(2)} & \mathbf{0}_{4\times4} & \mathbf{0}_{4\times4} \\ \mathbf{A}_{1(6)} & \mathbf{0}_{4\times4} & \mathbf{A}_{2(6)} & \mathbf{0}_{4\times4} \\ \mathbf{A}_{1(12)} & \mathbf{0}_{4\times4} & \mathbf{0}_{4\times4} & \mathbf{A}_{2(12)} \end{bmatrix}, \quad \mathbf{x}_{\mathrm{aug}} = \begin{bmatrix} \mathbf{x_0} \\ \mathbf{r}_{(2)} \\ \mathbf{r}_{(6)} \\ \mathbf{r}_{(12)} \end{bmatrix},$$

$$\mathbf{B}_{\mathrm{aug}} = \begin{bmatrix} \mathbf{B} \\ \mathbf{0}_{14\times2} \end{bmatrix}, \quad \mathbf{E}_{\mathrm{aug}} = \begin{bmatrix} \mathbf{E} \\ \mathbf{0}_{14\times2} \end{bmatrix}, \quad \mathbf{A}_0 = \begin{bmatrix} \mathbf{A} & \mathbf{0}_{2\times2} \\ -\mathbf{I}_{2\times2} & \mathbf{0}_{2\times2} \end{bmatrix},$$

$$\mathbf{A}_{1(h)} = -h\omega \begin{bmatrix} \mathbf{0}_{2\times2} & \mathbf{0}_{2\times2} \\ \mathbf{I}_{2\times2} & \mathbf{0}_{2\times2} \end{bmatrix}, \quad \mathbf{A}_{2(h)} = h\omega \begin{bmatrix} \mathbf{0}_{2\times2} & \mathbf{I}_{2\times2} \\ -\mathbf{I}_{2\times2} & \mathbf{0}_{2\times2} \end{bmatrix}$$

and

$$\mathbf{x_0} = \begin{bmatrix} i_d^{\mathrm{m}} & i_q^{\mathrm{m}} & p_d & p_q \end{bmatrix}^{\mathrm{T}}, \quad \mathbf{r}_{(h)} = \begin{bmatrix} r_{1d}^{(h)} & r_{1q}^{(h)} & r_{2d}^{(h)} & r_{2q}^{(h)} \end{bmatrix}^{\mathrm{T}}$$

for $h = \{2, 6, 12\}$. The subscript $_{\mathrm{aug}}$ corresponds to matrices describing the augmented system.

In order to design the full state-feedback current controller the `lqrd` MATLAB®'s function is applied [45]. This function calculates the matrix $\mathbf{K}_{\mathrm{aug}}$ for digital implementation where the

state-feedback law $\mathbf{u}(k) = -\mathbf{K}_{\text{aug}}\mathbf{x}_{\text{aug}}(k)$ minimizes the discrete cost function equivalent to the continuous one:

$$J = \int_0^\infty \left(\mathbf{x}_{\text{aug}}^{\text{T}}\mathbf{Q}_{\text{aug}}\mathbf{x}_{\text{aug}} + \mathbf{u}^{\text{T}}\mathbf{R}\mathbf{u}\right) \mathrm{d}t\,, \tag{6}$$

where $\mathbf{Q}_{\text{aug}}$ and $\mathbf{R} = \texttt{diag}([r,r])$, are weighting matrices. Scaling of $\mathbf{Q}$ and $\mathbf{R}$ by the same factor does not change the extrema of the cost function. Thus, it is important to define $\mathbf{Q}$ matrix in relation to r. As a consequence, in this study $\mathbf{R}$ is an identity matrix $\mathbf{R} = \mathbf{I}$ and only $\mathbf{Q}$ is subjected to tuning problem.

It was assumed, that the same penalty weights are applied in both d and q axes of the current control structure. Accordingly, weighting matrices are presented as follows:

$$\mathbf{Q_{aug}} = \begin{bmatrix} \mathbf{Q_0} & \mathbf{0} & \mathbf{0} & \mathbf{0} \\ \mathbf{0} & \mathbf{Q_{r(2)}} & \mathbf{0} & \mathbf{0} \\ \mathbf{0} & \mathbf{0} & \mathbf{Q_{r(6)}} & \mathbf{0} \\ \mathbf{0} & \mathbf{0} & \mathbf{0} & \mathbf{Q_{r(12)}} \end{bmatrix} \tag{7}$$

where $\mathbf{Q_0} = \texttt{diag}([q\ q\ q_p\ q_p])$ and where $\mathbf{Q_{r(h)}} = \texttt{diag}\left(\left[r_{1d}^{(h)}\ r_{1q}^{(h)}\ r_{2d}^{(h)}\ r_{2q}^{(h)}\right]\right)$ for $h = \{2,6,12\}$.

The penalty weights are selected in the PSO procedure.

2.2. Particle swarm optimization. Particle swarm optimization is a metaheuristic gradientless method that employs a set of virtual particles, called a swarm, to find a solution. The particles are moving over a multidimensional space. The number of dimensions is defined by the number of parameters to be found. Thus, the particles' coordinates in the search-space are a candidate solution of the optimization problem. In the case discussed in this paper, the resulting search space is five-dimensional according to (7), i.e. there is a need to determine values of the following parameters: q, q_p, $q_r^{(2)}$, $q_r^{(6)}$ and $q_r^{(12)}$. However, in this study, the sought parameters ρ_i in the optimization process are the exponents of 10 rather than the direct values of $\mathbf{Q}_{\text{aug}}$ matrix entries. The selection of exponents facilitates the tuning process and it is a common approach for LQR [46, 47]. Thus, the $\mathbf{Q}_{\text{aug}}$ entries correspond to ρ_i as follows:

$$q = 10^{\rho_1}\,, \qquad q_p = 10^{\rho_2}\,, \qquad q_r^{(2)} = 10^{\rho_3}\,,$$
$$q_r^{(6)} = 10^{\rho_4}\,, \qquad q_r^{(12)} = 10^{\rho_5}\,.$$

The initial positions of the particles are randomised (Fig. 3a). Then, in an iterative manner, all potential solutions determined by the current position of the particles are evaluated and next a new position of each particle is determined. The change in position over one iteration is velocity. Particle velocity in a given iteration is determined on the basis of its outgoing velocity and also on the basis of the so far best solutions found by a given particle and by all particles in the swarm. The rules for updating the swarm are described by the following equations:

$$v_i^j(k+1) = c_1 v_i^j(k) + c_2 r_1 \left(x_i^j(k_{\text{best}}^j) - x_i^j(k)\right) + \\ + c_2 r_2 \left(x_i^{j_{\text{best}}}\left(k_{\text{best}}^{j_{\text{best}}}\right) - x_i^j(k)\right), \tag{8}$$

$$x_i^j(k+1) = x_i^j(k) + v_i^j(k+1), \tag{9}$$

where $v_i^j(k)$ and $x_i^j(k)$ are respectively velocity and position in the i-th dimmension of the search-space for the j-th particle in the k-th iteration. While $x_i^j(k_{\text{best}}^j)$ represents the best so far found solution of a given particle and j_{best} is the index of the global best particle, that is selected from the swarm after each iteration. Weighting coefficients c_1, c_2, c_3 are constant and are called the inertia, cognitive and social coefficient, respectively. In this study, these coefficients were determined on the basis of the typical formula for PSO algorithms [48, 49] and are as follows: 0.73, 1.5 and 1.5. Variables r_1 and r_2 are random numbers with a uniform distribution in the range $\langle 0, 1\rangle$. The velocity component associated with the global best position in equation (8) causes the swarm to gradually converge around the found optimum. When a stopping condition is met, the optimization

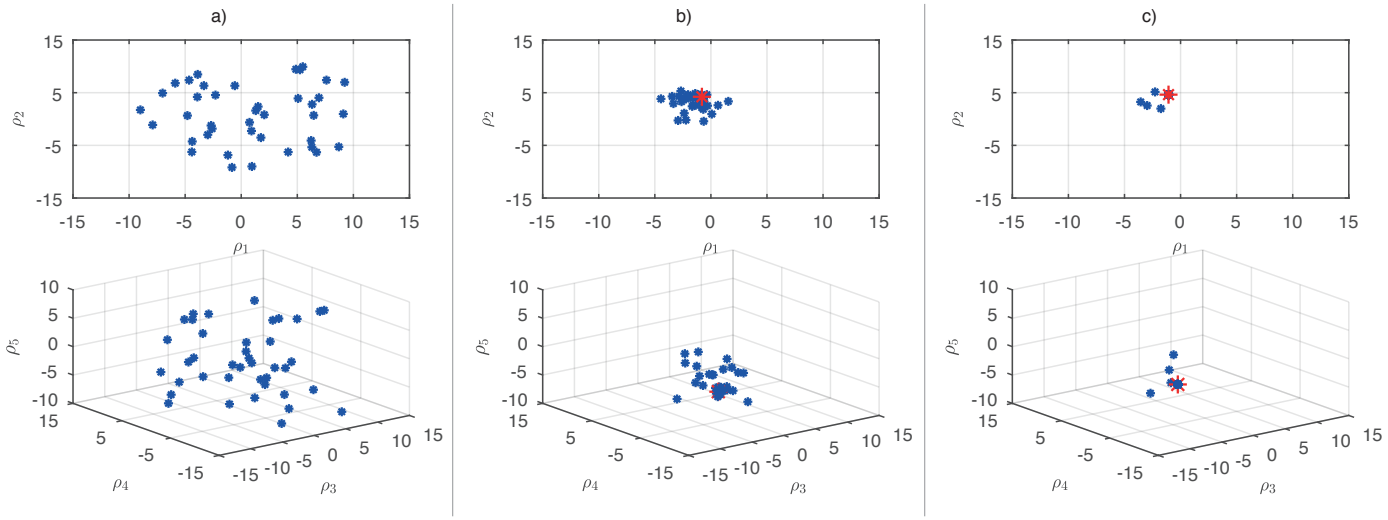

Fig. 3. Initial particles positions (a), positions after the 20th (b) and 100th (c) iteration

is completed and the vector $x^{j_{\text{best}}}(k^{j_{\text{best}}}_{\text{best}})$ represents the final solution found by the swarm.

The diagram of the numerical model applied for the optimization is presented in Fig. 2. The crucial issue that influences the quality of the obtained results is the selection of an appropriate objective function and the test cycle in which this function is calculated. The conditions describing the test cycle are the disturbance and reference signals.

Considering the current control loop of the AC/DC converter, the disturbance is the grid voltage. The profile of the grid voltage in the rotating reference is presented in Fig. 4. A portion of the grid voltage waveform in the stationary reference frame is shown in Fig. 5. In the time intervals 0–0.1 s and 0.9–1.0 s three phase sinusoidal and symmetrical voltage is applied. In order to excite the oscillatory terms in the control structure higher voltage harmonics are included in voltage grid signals in the period 0.1–0.9 s. For the same purpose, voltage sag and voltage unbalance are incorporated in the periods 0.3–0.4 s and 0.7–0.8 s. The reference signals for the test cycle are presented in Fig. 6. The shape of the reference signal is obtained from a rectangular pulse generator and the first-order lag system connected in series. In that way the frequency bandwidth of the reference signal is limited. It corresponds with the dynamics of the reference signal in real system that is, in the presented control system, indirectly limited by DC-link capacitance.

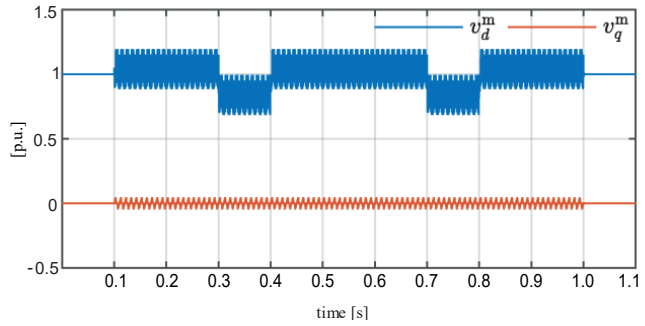

Fig. 4. v_d^{m}, v_q^{m} voltage components in the test cycle

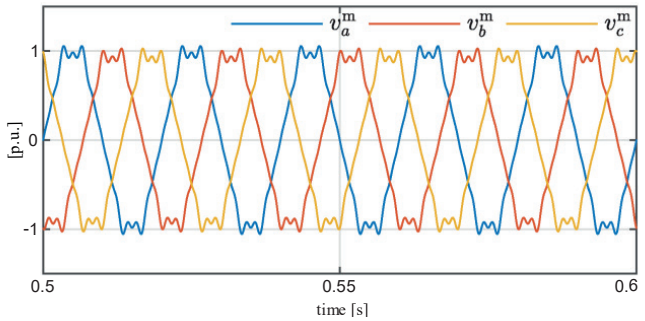

Fig. 5. Distorted grid voltage waveform in the test cycle

The selected objective function bases on the integral square error index and is given as follows:

$$J_{\text{pso}} = \sum_{k=0}^{N} \mathbf{e}(k)^{\text{T}} \mathbf{e}(k)\,. \tag{10}$$

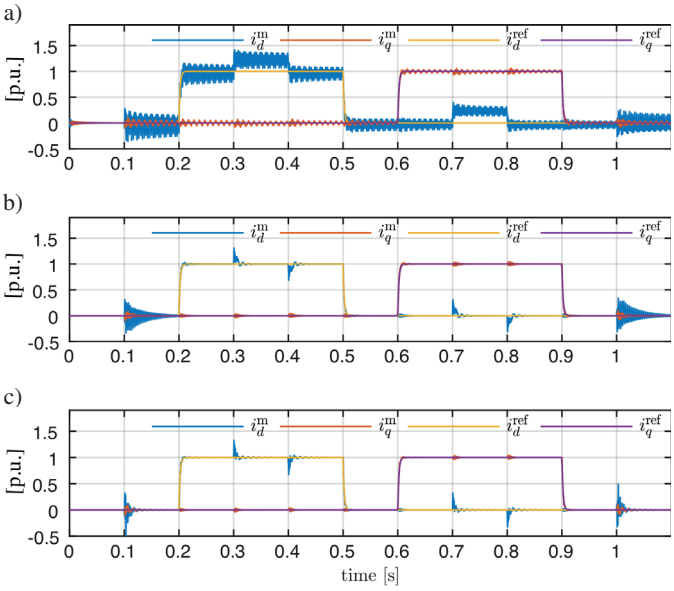

Fig. 6. i_d^{m}, i_q^{m} current components in the simulation test for the best solution after 5th (a), 20th (b) and 100th (c) iteration

Of note here is that theoretically possible full access to $\mathbf{Q}_{\text{aug}}$ by PSO means that the control effort is not taken into account. Because of unavoidable identification errors and measurement noise, the found solution may turn out to be unstable in a real system, if the control effort is neglected. It causes that some restrictions on the control signal in the dynamic state are required. It can be performed in many ways. In the study presented in [29] the penalty function has been added to the objective function. This method comes with a drawback, because the new element in performance index needs a subjective weight that has to be set by guessing and checking. In this study, the adjustment of reference signal has been proposed to penalize too aggressive control behaviour. The desired dynamic of the current control loop is directly defined by the reference signal in the test cycle and there is no need to use a combined performance index. The reference signals are shaped using the low-pass filter LPF_{ref} as presented in Fig. 2. This filter is used only at the optimization stage. In the full control system, that is implemented in the converter platform, the reference current signal i_d^{ref} is generated by the PI DC-link voltage controller.

It is important to identify delays in the current control loop. In this study it was done in accordance with [50], therefore the total delay time T_{total} is as follows:

$$T_{\text{total}} = T_{\text{mc}} + T_{\text{PWM}} + T_{\text{aver}}\,, \tag{11}$$

where T_{mc} is the processing delay of microcontorller and equals switching period T_{s}, $T_{\text{PWM}} = 0.5T_{\text{s}}$ is the delay time associated with modulation technique, $T_{\text{aver}} = 0.5T_{\text{s}}$ is the time linked with additional averaging filter in the feedback loop. Thus, the total delay in the system is $2T_{\text{s}}$ and is modeled as z^{-2} in the discrete time domain.

More details on $\mathbf{N}$ calculation for current controller of grid-connected converter has been presented in our previous work [31].

Optimization is performed offline based on the numerical model in MATLAB environment. Because of using a parallel computing approach to run the optimization process [51], the number of particles was selected as a multiple of the number of CPU cores. In our study eight cores were used and the swarm consisted of 40 particles. The optimization process was stopped after 100 iterations and the course of the optimization processes is presented in Figs 3 to 6. Exemplary states illustrating the particles' position in the search space are presented in Fig. 3. The red marker denotes the best position found so far. After 100 iterations (Fig. 3c) 90% of all particles are usually in a radius of 0.05 from the global best position, taking into account all dimensions of the search-space. The other particles, that are more distant from the best position, are not converging intensively because of a long distance between global best position and their personal best position. It should be noted that very high convergence of the swarm, often observed for many PSO applications, is not necessary. The weak convergence of some particles does not affect the quality of the final solution. The change over iterations of the performance index J_{pso} for the global best solution is presented in Fig. 8. The value of sought parameters proposed by the swarm after each iteration is presented in Fig. 9. Big changes from one iteration to the next iteration in the parameter value, which are not typical for gradient methods, are characteristic of PSO and result from a change of the particle that represents the global best solution. The improvement of the current response for the best so far found solution over the optimization progress is illustrated in Fig. 6 and Fig. 7. There is a clear trend of decreasing the higher harmonics content in line with optimization progress.

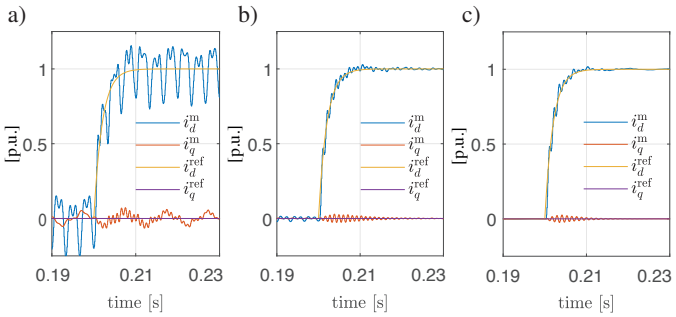

Fig. 7. Zoom on the waveforms from Fig. 6 in the range from 0.19 s to 0.23 s

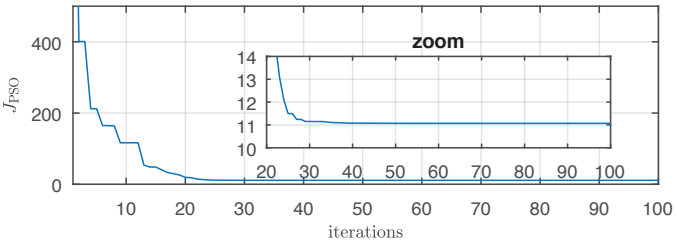

Fig. 8. Evolution of the performance index

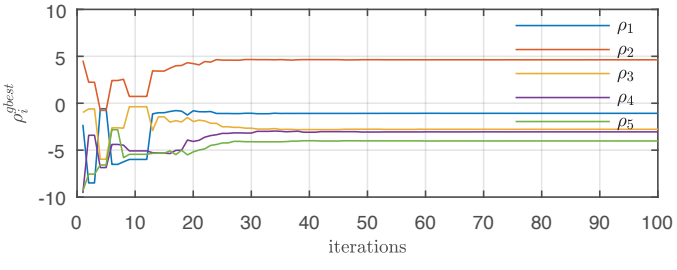

Fig. 9. The best set of parameters ρ_i found during the optimization process

2.3. DC-link voltage controller The PI controller with the clamping anti–windup mechanism is used in the outer control loop in the d axis to control DC-link voltage. The notch filter ($\text{NF}_{2\omega}$) is used to attenuate interference of double grid frequency in case of operating under unbalanced grid voltage conditions. The central rejected frequency is 100 Hz. Due to the fact that the DC-link voltage signal has higher harmonics and measurement noise the low-pass filter (LPF) is used. The design of the voltage controller is performed after the completion of the current controller design. For the purpose of voltage controller design, the dynamic of the inner current control loop in the d axis is approximated by the first order lag transfer function.

$$G_{\text{inner}} = \frac{1}{T_{\text{inner}} s + 1}. \tag{12}$$

The transfer function of the controller is as follows:

$$G_{\text{PI}} = \frac{K_{rv}(T_{rv} s + 1)}{T_{rv} s}. \tag{13}$$

Based on the equation describing the dynamics of v_{DC}:

$$\frac{\text{d}}{\text{d}t} v_{\text{dc}} = \frac{1}{C_{\text{dc}}} \left(\frac{3}{2} u_d i_d + \frac{3}{2} u_q i_q - i_{\text{load}} \right). \tag{14}$$

assuming $i_{\text{q}} = 0$ and the mentioned simplification of the current control loop, the voltage control loop is considered for the design purpose in the form presented in Fig. 10.

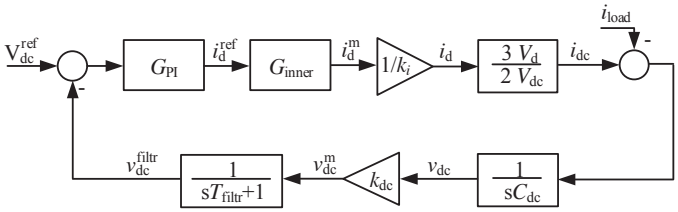

Fig. 10. Simplified control scheme for a grid-tied converter

Using the symmetrical optimum method for the tuning of voltage controller, the parameters of the PI controller are expressed as follows [52]:

$$K_{rv} = \frac{2}{3} \frac{C_{\text{dc}}}{\alpha \tau} \frac{V_{dc}}{V_{\text{d}}} \frac{k_{\text{dc}}}{k_{\text{i}}}, \tag{15}$$

$$T_{rv} = \alpha^2 \tau, \tag{16}$$

where $\tau = T_{\text{inner}} + T_{\text{filtr}}$ and $\alpha = 2$.

3. Experimental study

The performance of the control system, designed using the proposed method for the grid-tied converter has been verified in experimental tests using 10 kW laboratory setup presented in Fig. 11. Parameters of the system are presented in Table 1. Physical experiment results presented in this section were recorded by oscilloscopes in digital form. In the laboratory setup two three-phase voltage source converters with common DC circuit have been used. The first one is operated as grid-side converter and the second one was used an active load. Both converters are controlled by a control board with TMS 320F28335 microcontorller. The calculations related to the implemented oscillatory terms for pulsations $2\omega, 6\omega, 12\omega$ take 2.1 µs. It imply the compensation of several harmonics is not an excessive computational burden for the converter operating with 10 kHz switching frequency and overall time available for calculation of 100 µs. The implementation details are presented in [6].

Fig. 11. Laboratory setup

Table 1
Parameters of the experimental setup with the grid-tie converter

Symbol	Value	Description
V_{dc}	700 V	Nominal DC–link voltage
V	400 V	Nominal input voltage RMS value
ω	100π s^{-1}	Nominal pulsatance of the input voltage
L	2 mH	Inductances of the input filter
R	0.2 Ω	Resistances of the input filter
C	1.5 mF	Capacitance of the DC–link capacitor
P_n	10 kW	Nominal power
F_s	10 kHz	Switching/sampling frequency
k_{dc}	1/700	DC–link voltage scaling factor
k_i	1/20.5	Current scaling factor

To highlight the contribution of oscillatory terms, first, the results for the control structure without oscillatory terms are presented in Fig. 12. The design and the optimization process were performed analogously to the procedure presented in previous sections, with the difference that the augmentation contains only integral terms. This result expressly shows how asymmetry and higher harmonics components of grid voltage affect grid current. The voltage higher harmonics contribution is as follows: 5th – 4%, 7th – 1.6%, 11th – 1%, 13th – 0.5% and the current harmonics contribution is 9.7%, 4.8%, 3.2%, 1.9% respectively. The obtained results explain the motivation to expand the control structure by oscillatory terms. The mathematical justification for such a decision results from the internal model principle.

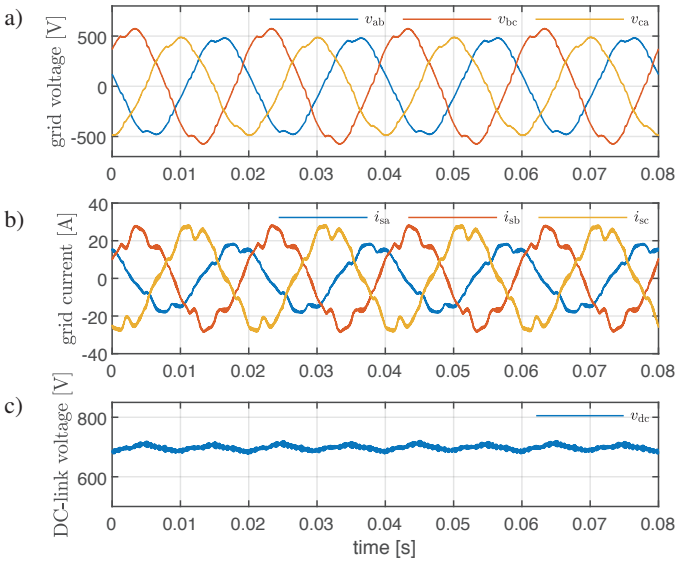

Fig. 12. Operation of the grid converter without oscillatory terms under asymmetrical and distorted voltage condition

The next presented results concern the described control structure with the oscillatory terms (Fig. 1). Fig. 13 presents operation under the distorted voltage condition for a suddenly change of the load. In the period from 0.013 s to 0.137 s the nominal load was applied to the DC side. THD of the grid voltage is 8%. In the steady state under the load condition, the THD of the grid current is 2%. This case shows the performance of the control structure in terms of output voltage stabilization and providing the sinusoidal grid current.

The response of the system to load changes has meet our expectations. However, in this case, due to the dynamics of voltage changes in the DC circuit, even step changes of load current are unable to greatly actuate the current controller in the range of higher frequencies. In the next tests, a change of grid voltage distortion was applied. Figs 14 and 15 show the transient states after a sudden increase and decrease of higher harmonics content in the grid voltage. The presented results demonstrate that the system is working properly and also handles disturbances that affect the current controller in the range of high frequencies. The rejection higher harmonics takes place ca. 1.5 of the period after the change.

In the next case (Fig. 16), apart from distortion of grid voltage, dynamic asymmetric voltage dip was applied. In the period from 0.05 s to 0.24 s, there is a voltage dip with a 15% share of the negative sequence component resulting in grid voltage asymmetry. The Fourier spectrum of grid voltages and currents for steady state during the asymmetrical dip is shown in Fig. 17.

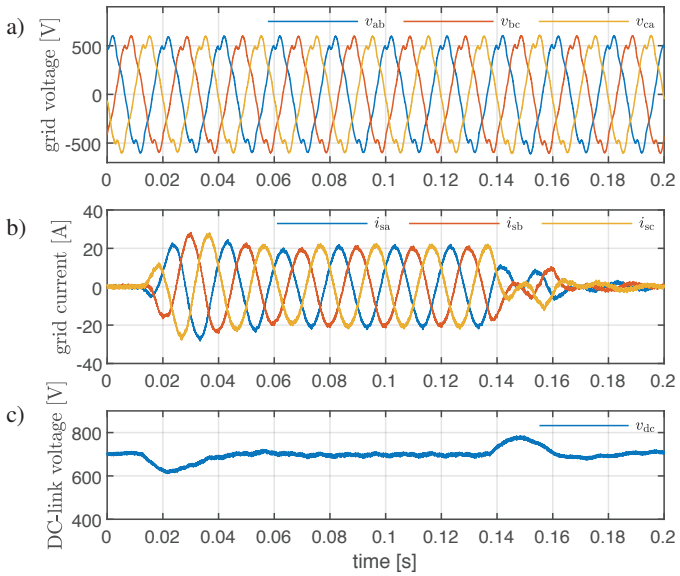

Fig. 13. Experimental results of grid converter operation under distorted voltage condition

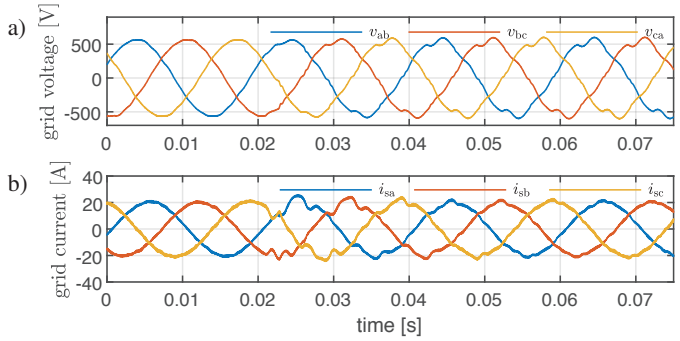

Fig. 14. Sudden increase in higher harmonics of grid voltage

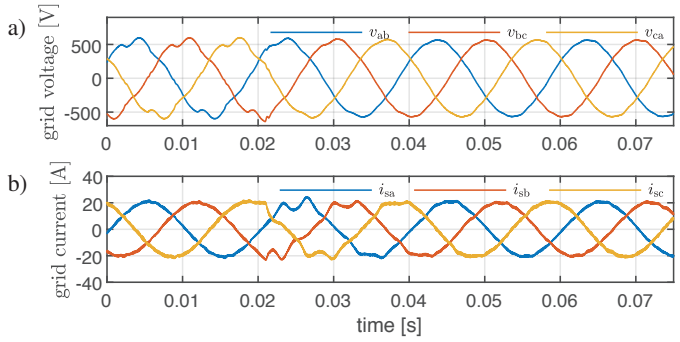

Fig. 15. Sudden decrease in higher harmonics of grid voltage

This case shows the ability of the presented control structure to provide symmetrical currents with a low content of higher harmonic under conditions of voltage distortion and asymmetry. Moreover, the analysis of the transient states (Fig. 16) has been addressed and the results should be assessed as in line with expectations. In the vicinity of 0.25 s, in addition to the temporary change in amplitude of fundamental harmonic, a short-term distortion of the current caused by higher order harmonics is noticeable. This is due to the temporary saturation of oscillatory terms in the current controller structure. Such a state does not cause any malfunction and the system returns freely to normal operation.

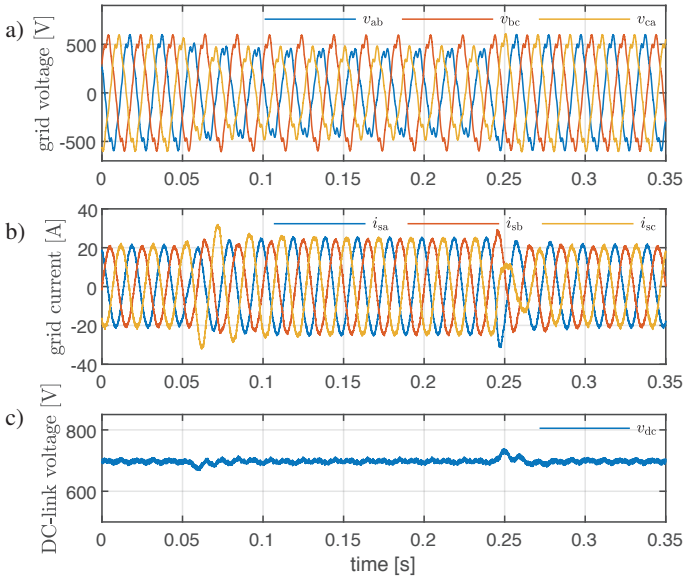

Fig. 16. Operation of the grid converter under asymmetrical voltage dip

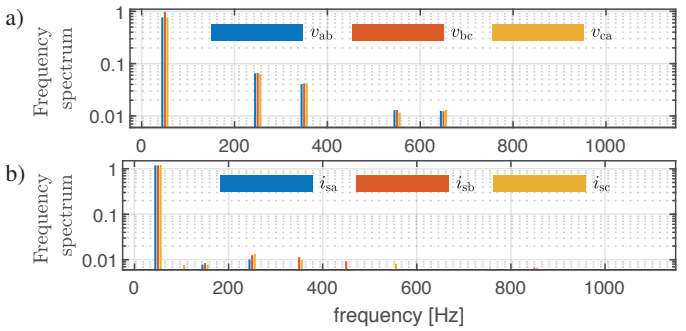

Fig. 17. Normalised frequency spectrum for unbalanced and distorted voltage conditions

4. Summary

This paper has investigated the LQR-based control system for the grid-tied converter. It has been demonstrated that the selection of weighting matrices in LQR can be effectively done using particle swarm optimization. The selection of weighting entries directly by the designer might be very onerous, especially for systems with a large number of state variables. The automated method presented in this study allows to deal with this problem in an accessible way. The original pattern of the optimization configuration including selection of i.a. the cost function, the search-space domain, the numerical model and the test cycle is proposed. The developed test cycle is takes into account all crucial types of disturbances as voltage unbalance, higher harmonics and voltage dip. The experimental study has been conducted

to evaluate the performance of the designed system. It is worthwhile noting that experimental study includes a lot of dynamic states. This fact is of particular importance for control structures with oscillatory terms, because in dynamic states they are susceptible to an excessive stimulation and loss of stability. For this reason, tuning of such a control structure is not intuitive. The presented procedure of designing the linear-quadratic current controller for the three-phase grid-tied converter leads to satisfactory results concerning not only steady states but also various types of transient states.

Acknowledgements. The research was supported by the National Centre for Research and Development (Narodowe Centrum Badan i Rozwoju) within the project No. PBS3/A4/13/2015 entitled "Superconducting magnetic energy storage with a power electronic interface for the electric power systems" (original title: "Nadprzewodzący magazyn energii z interfejsem energoelektronicznym do zastosowań w sieciach dystrybucyjnych"), 01.07.2015–31.12.2018. The acronym for the project is NpME.

References

[1] M. Malinowski, M. Jasiński, and M.P. Kaźmierkowski, "Simple direct power control of three-phase PWM rectifier using space-vector modulation (DPC-SVM)", *IEEE Trans. Ind. Electron.* 51 (2), 447–454, (2003).

[2] M. Bobrowska-Rafal, K. Rafal, G. Abad, and M. Jasinski, "Control of PWM rectifier under grid voltage dips", *Bull. Pol. Ac.: Tech.* 57 (4), 337–343 (2009).

[3] M. Liserre, R. Teodorescu, and F. Blaabjerg, "Multiple harmonics control for three-phase grid converter systems with the use of PI-RES", *IEEE Trans. Pow. Electron.* 21 (3), 836–841 (2006).

[4] R. Teodorescu, M. Liserre, and P. Rodriguez, *Grid converter for photovoltaic and wind power systems*, John Wiley & Sons, New York, 2011.

[5] M. Jasiński, G. Wrona, and Sz. Piasecki, "Control of Grid Connected Converter (GCC) Under Grid Voltage Disturbances", *Advanced and Intelligent Control in Power Electronics and Drives*, 91–142 (2014).

[6] K. Jackiewicz, A. Stras, B. Ufnalski, and L.M. Grzesiak, "Comparative study of two repetitive process control techniques for a grid-tie converter under distorted grid voltage conditions", *Int. J. Electr. Power Energy Syst.* 113, 64–175 (2019).

[7] D. Zieliński, P. Lipnicki, and W. Jarzyna, "Synchronization of voltage frequency converters with the grid in the presence of notching", *COMPEL: The International Journal for Computation and Mathematics in Electrical and Electronic Engineering* 34 (3), 657–673 (2015).

[8] CENELEC: European Committee for Electrotechnical Standardization, "Voltage Characteristics of Public Distribution System", Brussels, Belgium, 1999.

[9] Intern. Electrotechnical Commission, "IEC 61000-3-2 Electromagnetic Compatibility (EMC) – Part 3-2: Limits for Harmonic current Emissions (Equipment Input Current $\leq$ 16 A per phase", Geneva, Switzerland, 2018.

[10] Intern. Electrotechnical Commission, "IEC 61000-3-12 Electromagnetic Compatibility (EMC)–Part 3-12: Limits for Harmonic current Emissions (Equipment Input Current $>$ 16 A and $\leq$ 75 A per phase", Geneva, Switzerland, 2018.

[11] D. Priyanga and N.K. Jisi, "Repetitive Controller Based Grid Current Compensator for Distributed Generation", *International Journal of Computer Science and Engineering Communications* 5 (3), 1556–1565 (2017).

[12] Q.N. Trinh, P. Wang, Y. Tang, and F.H. Choo, "Mitigation of DC and Harmonic Currents Generated by Voltage Measurement Errors and Grid Voltage Distortions in Transformerless Grid-Connected Inverters", *IEEE Trans. Energy Convers.* 33 (2), 801–813 (2018).

[13] C. Blanco, F. Tardelli, D. Reigosa, P. Zanchetta, and F. Briz, "Design of a Cooperative Voltage Harmonic Compensation Strategy for Islanded Microgrids Combining Virtual Admittance and Repetitive Controller", *IEEE Trans. Ind. Appl.* 55 (1), 680–688 (2019).

[14] B. Ufnalski, L.M. Grzesiak, A. Kaszewski, and A. Galecki, "On the similarity and challenges of multiresonant and iterative learning current controllers for grid converters and why the disturbance feedforward matters", *Przeglad Elektrotechniczny (Electrical Review)* 94 (5/2018), 38–46 (2018).

[15] G. Iwanski, T. Luszczyk, and M. Szypulski, "Virtual-Torque-Based Control of Three-Phase Rectifier Under Grid Imbalance and Harmonics", *IEEE Trans. Pow. Electron.* 32 (9), 6836–6852 (2017).

[16] G. Iwanski, "Virtual Torque and Power Control of a Three-Phase Converter Connected to an Unbalanced Grid With Consideration of Converter Current Constraint and Operation Mode", *IEEE Trans. on Power Electr.* 34 (4), 3804–3818 (2019).

[17] P. Falkowski and A. Sikorski, "Finite control set model predictive control for grid-connected AC–DC converters with LCL filter", *IEEE Trans. Ind. Electron.* 65 (4), 2844–2852 (2017).

[18] J.A. Rohten, J.R. Espinoza, J.A. Muñoz, M.A. Pérez, P.E. Melin, J.J. Silva, E.E. Espinosa, and M.E. Rivera, "Model predictive control for power converters in a distorted three-phase power supply", *IEEE Trans. Ind. Electron.* 63 (9), 5838–5848 (2016).

[19] J. Kukkola, M. Hinkkanen, and K. Zenger, "Observer-Based State-Space Current Controller for a Grid Converter Equipped With an LCL Filter: Analytical Method for Direct Discrete-Time Design", *IEEE Trans. Ind. Appl.* 51 (5), 4079–4090 (2015).

[20] C. Xie, X. Zhao, K. Ki, D. Liu, J.M. Guerrero, and J.C. Vasquez, "Phase Compensated Reduced Order Generalized Integrators for Grid-Tied VSCs With Harmonics Compensation Capability", *IEEE Trans. Ind. Appl.* 54 (3), 2568–2578 (2018).

[21] D. Pérez-Estévez, J. Doval-Gandoy, A.G. Yepes, Ó. López, and F. Baneira, "Generalized Multifrequency Current Controller for Grid-Connected Converters With LCL Filter", *IEEE Trans. Ind. Appl.* 54 (5), 4537–4553 (2018).

[22] C.A. Busada, S.G. Jorge, and J.A. Solsona, "Full-State Feedback Equivalent Controller for Active Damping in LCL-Filtered Grid-Connected Inverters Using a Reduced Number of Sensors", *IEEE Trans. Ind. Electron.* 62 (10), 5993–6002 (2015).

[23] F. Huerta Sánchez, J. Pérez, S. Cobreces Alvarez, and M. Rizo, "Frequency-Adaptive Multi-Resonant LQG State-Feedback Current Controller for LCL-Filtered VSCs under Dist. Grid Voltages", *IEEE Trans. Ind. Electron.* 65 (11), 8433–8444 (2018).

[24] K.J. Aström and R.M. Murray, *Feedback systems: An Introduction For Scientists and Engineers*, Princeton University Press, 2010.

[25] M. Szypulski and G. Iwański, "Synchronization of state-feedback-controlled doubly fed induction generator with the grid", *Bull. Pol. Ac.: Tech.* 66 (5), 675–685 (2018).

[26] A. Douik, L. Hend, and H. Messaoud "Optimised Eigenstructure Assignment by Ant System And LQR Approaches.", *Int. J. Adv. Comput. Sci. Appl.* 5 (4), 45–56 (2008).

[27] T. Tarczewski and L.M. Grzesiak, "Application of artificial bee colony algorithm to auto-tuning of linear-quadratic regulator for PMSM position control", *Przeglad Elektrotechniczny (Electical review)* 92 (6), 57–62 (2016).

[28] S.A. Ghoreishi and M.A. Nekoui, "Optimal weighting matrices design for LQR controller based on genetic algorithm and PSO", *Advanced Materials Research* 433, 7546–7553 (2012).

[29] B. Ufnalski, A. Kaszewski, and L.M. Grzesiak, "Particle Swarm Optimization of the Multioscillatory LQR for a Three-Phase Four-Wire Voltage-Source Inverter With an LC Output Filter", *IEEE Trans. Ind. Electron.* 62 (1), 484–493 (2015).

[30] A. Demiroren and M. Guleryuz, "PSO algorithm-based optimal tuning of STATCOM for voltage control in a wind farm integrated system", *Int. Conf. Electr. Electron. Eng., 7th*, 367–370 (2011).

[31] A. Galecki, A. Kaszewski, B. Ufnalski, and L.M. Grzesiak, "State current controller with oscillatory terms for three-level grid-connected PWM rectifiers under distorted grid voltage conditions", *Proc. Int. Conf EPE-ECCE Europe*, 1–10 (2015).

[32] A. Gałecki, L. Grzesiak, B. Ufnalski, A. Kaszewski, and M. Michalczuk, "Anti-windup strategy for an LQ current controller with oscillatory terms for three-phase grid-tie VSCs in SMES systems", *Power Electronics and Drives* 1 (2), 65–81 (2016).

[33] A. Galecki, L. Grzesiak, B. Ufnalski, A. Kaszewski, and M. Michalczuk, "Multi-oscillatory current control with anti-windup for grid-connected VSCs operated under distorted grid voltage conditions", *Proc. Int. Conf EPE-ECCE Europe*, 1–10 (2017).

[34] A. Galecki, A. Kaszewski, L.M. Grzesiak, and B. Ufnalski, "Particle swarm optimization of the multioscillatory LQR for a three-phase grid-tie converter", *Przeglad Elektrotechniczny (Electrical Review)* 94 (6/2018), 43–48 (2018).

[35] B. Ufnalski and L.M. Grzesiak, "Plug-in direct particle swarm repetitive controller with a reduced dimensionality of a fitness landscape–a multi-swarm approach", *Bull. Pol. Ac.: Tech.* 63 (4), 857–866 (2015).

[36] B. Ufnalski, L.M. Grzesiak, and K. Gałkowski, "Particle swarm optim. of an iter. learning controller for the single-phase inverter with sinusoidal output voltage waveform", *Bull. Pol. Ac.: Tech.* 61 (3), 649–660 (2013).

[37] M. Safonov and M. Athans, "Gain and phase margin for multiloop LQG regulators", *IEEE Trans. Autom. Control* 22 (2), 173–179 (1977).

[38] W.S. Levine, *The Control Systems Handbook: Control System Advanced Methods*, CRC press, 2010.

[39] Zwe-Lee Gaing, "A particle swarm optimization approach for optimum design of PID controller in AVR system", *IEEE Trans. Energy Convers.* 19 (2), 384–391 (2004).

[40] M.P. Kaźmierkowski, R. Krishnan, and F. Blaabjerg, *Control in Power Electronics*, Academic Press, 2002.

[41] Yi Fei Wang and Yun Wei Li, "Grid Synchronization PLL Based on Cascaded Delayed Signal Cancellation", *IEEE Trans. Pow. Electron.* 26 (7), 1987–1997 (2011).

[42] Y. Yang, K. Zhou, and F. Blaabjerg, "Enhancing the Frequency Adaptability of Periodic Current Controllers With a Fixed Sampling Rate for Grid-Conn. Power Conv.", *IEEE Trans. Pow. Electron.* 31 (10), 7273–7285 (2016).

[43] M.P. Kaźmierkowski, M. Jasiński, and G. Wrona, "DSP-Based Control of Grid-Connected Power Converters Operating Under Grid Distortions", *IEEE Trans. Ind. Informatics* 7 (2), 204–211 (2011).

[44] K. Zhou, Y. Yang, F. Blaabjerg, and D. Wang, "Optimal Selective Harmonic Control for Power Harmonics Mitigation", *IEEE Trans. Ind. Electron.* 62 (2), 1220–1230 (2015).

[45] Matlab, Design discrete linear-quadratic LQ regulator for continuous plant, https://www.mathworks.com/help/control/ref/lqrd.html, 2018, 2020-01-16.

[46] T. Duriez, S.L. Brunton, and B.R. Noack, "Methods of Linear Control Theory", *Machine Learning Control – Taming Nonlinear Dynamics and Turbulence*, Springer, 49–68 (2017).

[47] B. Kedjar and K. Al-Haddad, " LQ control of a three-phase four-wire shunt active power filter based on three-level NPC inverter", *Proc. Int. Conf. CCECE* 1297–1302 (2008).

[48] R.C. Eberhart and Yuhui Shi "Comparing inertia weights and constriction factors in particle swarm optimization", *Proc. of the IEEE Congres CEC*, 1, 84–88 (2000).

[49] M. Clerc and J. Kennedy, "The particle swarm-explosion, stability, and convergence in a multidimensional complex space", *IEEE Trans. Evol. Comput.* 6 (1), 58–73 (2002).

[50] V. Blasko, V. Kaura, and W. Niewiadomski, "Sampling of discontinuous voltage and current signals in electrical drives: a system approach", *IEEE Trans. Ind. Appl.* 34 (5), 1123–1130 (1998).

[51] M. Michalczuk, "On-line: Particle Swarm Optimization using parallel computing", *https://www.mathworks.com/ matlabcentral/profile/ authors/3157172-marek-michalczuk*, 2020-01-16.

[52] J. Dannehl, Ch. Wessels, and F.W. Fuchs, "Limitations of voltage-oriented PI current control of grid-connected PWM rectifiers with LCL filters", *IEEE Trans. Ind. Electron.* 56 (2), 380–388 (2009).